

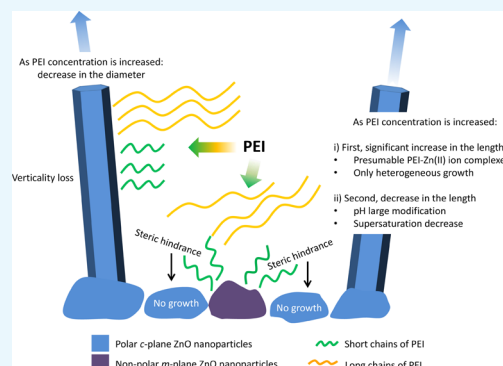
Effects of Polyethylenimine and Its Molecular Weight on the Chemical Bath Deposition of ZnO Nanowires

Romain Parize, Jérôme Daniel Garnier, Estelle Appert, Odette Chaix-Pluchery, and Vincent Consonni*

Univ. Grenoble Alpes, CNRS, Grenoble INP, LMGP, F-38000 Grenoble, France

Supporting Information

ABSTRACT: The addition of polyethylenimine (PEI) in the standard chemical bath deposition (CBD) of ZnO nanowires has received an increasing interest for monitoring their aspect ratio, but the physicochemical processes at work are still under debate. To address this issue, the effects of PEI are disentangled from the effects of ammonia and investigated over a broad range of molecular weight (i.e., chain length) and concentration, varying from 1300 to 750 000 and from 1.5 to 10 mM, respectively. It is shown that the addition of PEI strongly favors the elongation of ZnO nanowires by suppressing the homogeneous growth at the benefit of the heterogeneous growth as well as by changing the supersaturation level through a pH modification. PEI is further found to inhibit the development of the sidewalls of ZnO nanowires by adsorbing on their nonpolar *m*-planes, as supported by Raman scattering analysis. The inhibition proceeds even in the low pH range, which somehow rules out the present involvement of electrostatic interactions as the dominant mechanism for the adsorption. Furthermore, it is revealed that PEI drastically affects the nucleation process of ZnO nanowires on the polycrystalline ZnO seed layer by presumably adsorbing on the nanoparticles oriented with the *m*-planes parallel to the surface, reducing in turn their nucleation rate as well as inducing a significant vertical misalignment. These findings, specifically showing the effects of the PEI molecular weight and concentration, cast light onto its multiple roles in the CBD of ZnO nanowires.



INTRODUCTION

As a surface-scalable, low-cost, and low-temperature deposition technique,¹ chemical bath deposition (CBD) offers a powerful route to form ZnO nanowires (NWs) with high structural quality for their integration into a large number of nanoscale engineering devices.² To improve the performances of the present devices, it is typically required to thoroughly control the density and vertical alignment of ZnO NWs as well as their dimensions (i.e., length, diameter, and aspect ratio)² when homoepitaxially grown on a polycrystalline ZnO seed layer.³ The selective area growth approach using advanced lithography and etching in a cleanroom environment has a high potential,^{4,5} but its complexity and cost are not compatible with all the targeted technologies. Alternatively, following the spontaneous growth approach, the density and vertical alignment of ZnO NWs are basically governed by the respective density and mosaicity of the *c*-axis-oriented ZnO nanoparticles composing the polycrystalline ZnO seed layer.^{3,6,7} More recently, Cossuet et al. also revealed that some of the ZnO NWs with a vertical misalignment form on semipolar ZnO nanoparticles.⁸ In contrast, the dimensions of ZnO NWs are specifically driven by the chemicals in aqueous solution, including a zinc salt (e.g., zinc nitrate, zinc acetate, etc.) and a source of hydroxide ions [e.g., ethanol amine, hexamethylenetetramine (HMTA), NaOH, etc.].^{2,9} The heterogeneous formation of ZnO NWs proceeds according

to the following main chemical reaction:¹⁰ $\text{Zn}^{2+} + 2 \text{HO}^- \rightarrow \text{ZnO(s)} + \text{H}_2\text{O}$. To monitor the aspect ratio of ZnO NWs to a higher degree of precision, the introduction of chemical additives in aqueous solution acting as capping agents is of high interest. Polyethylenimine (PEI)^{11–13} and diamines like ethylenediamine^{14,15} adsorb on the nonpolar *m*-plane sidewalls of ZnO NWs to promote their axial elongation at the expense of the radial growth. In contrast, chlorine ions¹⁶ and citrate ions^{17,18} adsorb on the polar *c*-plane top facet of ZnO NWs to inhibit the axial elongation at the benefit of the radial growth. Joo et al. also reported the competitive and face-selective adsorption of non-zinc metal cations at a high pH to monitor the shape of ZnO nanostructures from platelets to needles.¹⁹ The present approach is highly dependent upon the pH via the involvement of specific electrostatic interactions²⁰ and further results in the doping of ZnO NWs following a thermal activation by annealing.²¹

In that context, the use of PEI has been reported to grow ZnO NWs with a large length as required for enhancing the performances of many devices including dye-sensitized solar cells.^{11–13} PEI exists in either a linear or a branched form, and its properties are strongly dependent upon that nature.^{22–27}

Received: July 13, 2018

Accepted: September 18, 2018

Published: October 2, 2018

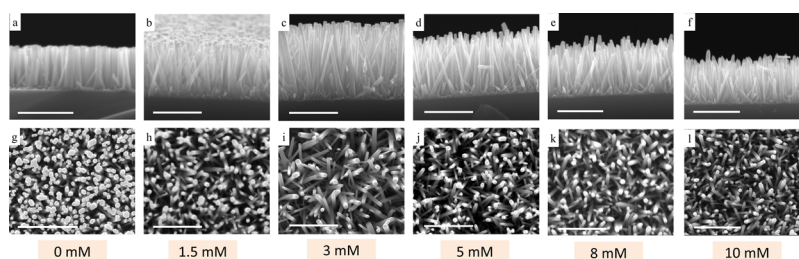


Figure 1. (a–f) Cross-sectional view and (g–l) top-view FESEM images of ZnO NWs grown by CBD with a PEI concentration in the range of 0–10 mM and for a given M_w of 1300. The scale bars represent 1 μm .

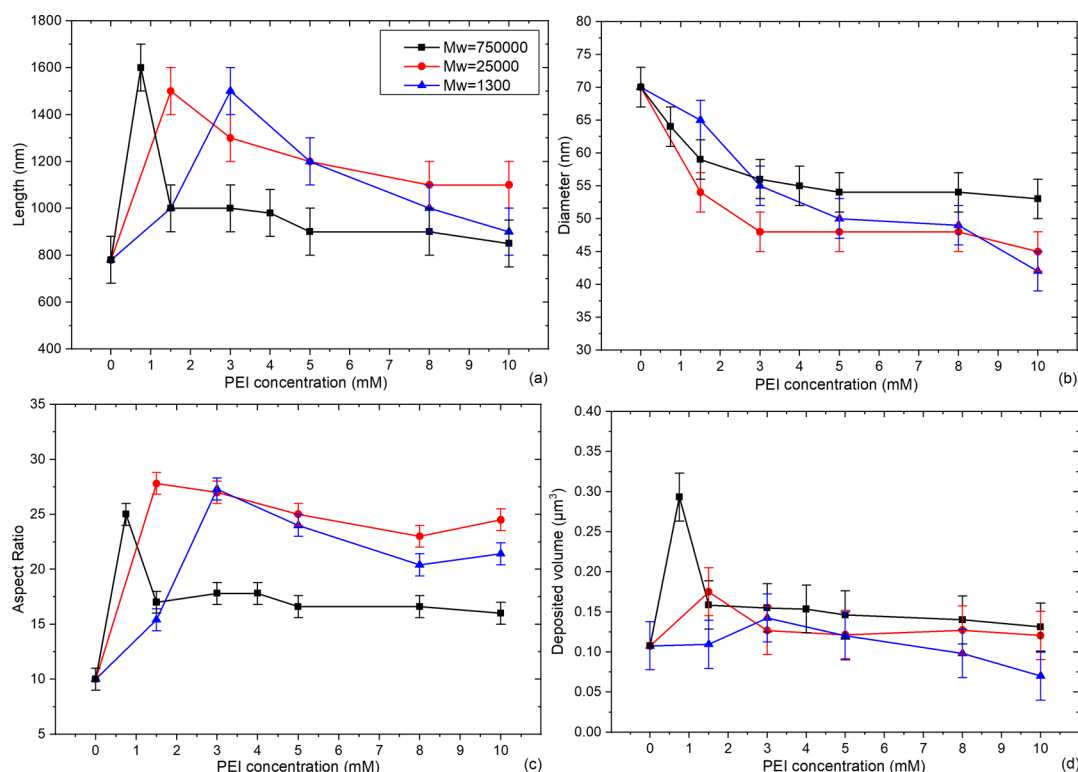


Figure 2. Evolution of the mean (a) length, (b) diameter, (c) aspect ratio, and (d) deposited volume of ZnO NWs grown by CBD as a function of the PEI concentration and for the given M_w of 1300, 25 000, and 750 000.

PEI in its more usual branched form is a nonpolar polymer consisting of an organic chain with the intercalations of N atoms and the ramifications of side amino groups ($-\text{NH}_2$).² It is positively charged over a broad range of pH, following the protonation of its side amino groups. The protonation rate is dependent upon the pH, reducing from 1 down to 0 in the pH range of 3–11.^{26,27}

It has been suggested that the adsorption of PEI on the sidewalls of ZnO NWs proceeds through the favorable electrostatic interactions between its protonated $-\text{NH}_2$ side groups and the negatively charged m -planes at a high pH above its isoelectric point (IEP) around 10.5,²⁸ but the present mechanism is still under debate. PEI has typically been used as the only chemical additive^{11,12,28–34} or with the combination of ammonia.^{13,34–40} Ammonia is often introduced in aqueous solution to increase the pH above 10.5 and to complete the action of PEI by further reducing the homogeneous nucleation.^{34–40} The role of ammonia is expected to complement the role of PEI to reach an even higher aspect ratio. However, at that high pH, the protonation rate is below 0.1, which directly questions the mechanisms at work for the

adsorption of PEI.^{26,27} The effects of PEI are thus much less pronounced at that high pH, and it is not straightforward to distinguish them from the effects of ammonia. Investigating the CBD of ZnO NWs with no ammonia, and thus at a lower pH, would enable to gain some crucial insights into the adsorption mechanisms at work.

The amount of PEI added in aqueous solution and the related pH are also expected to strongly affect the morphology of ZnO NWs. However, no comprehensive investigation stating the effects of the PEI concentration over a broad range or any study measuring the pH in an *in situ* manner have been reported. It has been shown that a relatively low concentration of PEI is able to strongly increase the aspect ratio of ZnO NWs,^{12,30,31} owing to its presumable coordination with Zn(II) ions^{35,41,42} limiting the homogeneous nucleation in aqueous solution at the benefit of the heterogeneous nucleation on the polycrystalline ZnO seed layer. This is also favorable to retain a relatively low pH to obtain a high protonation rate, but the potential electrostatic interactions are not favorable here as the m -planes are positively charged.

Furthermore, the effects of the molecular weight (M_w) of PEI, especially through its chain length, on the morphology of ZnO NWs, have never been investigated deeply, although it is expected to play a significant role. The use of PEI with the M_w of 800,^{13,37,40} 4000,²⁸ 4500,^{34,35} 25 000,⁴⁰ 70 000,²⁹ and 750 000³² has been reported, whereas many other reports did not notify it.^{11,12,30,31,33,36,38,39} The only investigation was achieved with the M_w of 800 and 25 000 using also ammonia, which somehow superimposes its effects and hence limits its impact on that specific aspect.⁴⁰ Investigating the CBD of ZnO NWs with the addition of PEI over a broad range of M_w would enable to understand in more detail its roles in aqueous solution.

In this paper, we disentangle the effects of PEI on the CBD of ZnO NWs using zinc nitrate and HMTA by introducing a varying concentration of PEI in the range of 1.5–10 mM and by measuring the pH in an in situ manner. The effects of the M_w (i.e., chain length) of PEI on the morphology of ZnO NWs are further investigated in detail to get a deeper insight into the physicochemical processes at work.

RESULTS

The structural morphology of ZnO NWs grown by CBD using the addition of PEI with the given M_w of 1300, 25 000, and 750 000 in a broad concentration range from 1.5 to 10 mM is shown by the cross-sectional view and top-view field emission scanning electron microscopy (FESEM) images in Figures 1, S1, and S2. It is clearly revealed that the morphology of ZnO NWs is strongly dependent upon the PEI concentration and M_w . The corresponding mean length, diameter, related aspect ratio, and deposited volume are presented in Figure 2 from the FESEM image analysis over a population of more than 200 ZnO NWs.

Effects of PEI on the Length and Deposited Volume of ZnO NWs. The evolutions of the length and deposited volume of ZnO NWs as a function of the PEI concentration for the given M_w of 1300, 25 000, and 750 000 are presented in Figure 2a,d. The length of ZnO NWs drastically increases from 780 ± 100 to about 1500 ± 100 nm in the low PEI concentration range and then decreases progressively, regardless of the M_w . Interestingly, the largest length is achieved for an optimal low PEI concentration, for which the value increases from 0.75 to 3 mM as the PEI M_w is decreased from 750 000 to 1300.

To account for the variation of the length of ZnO NWs, in situ pH measurements as a function of time are presented in Figure 3 for all the PEI concentrations and M_w . During the first 20 min, the pH is significantly reduced, as typically reported in refs 9, 20, 21. As the temperature of 60 °C is reached, HO^- ions are progressively released in aqueous solution, following the gradual hydrolysis of HMTA as a source of HO^- ions. This most likely accounts for the pH saturation after 20 min, which is further more pronounced as the PEI concentration is increased, regardless of its M_w . The growth temperature of 90 °C is reached after 40 min, which corresponds to the pH stabilization. The slight increase in the pH associated with the highest PEI concentration is likely due to the large consumption of Zn(II) ions acting as the limiting reactant species.⁹ In the present configuration with a large c -plane surface over the total surface ratio, the elongation of ZnO NWs is limited by the mass transport of the reactants and not by the surface reaction rate.^{43,44} The diffusive transport of Zn(II) ions acting as the limiting reactant in aqueous solution may

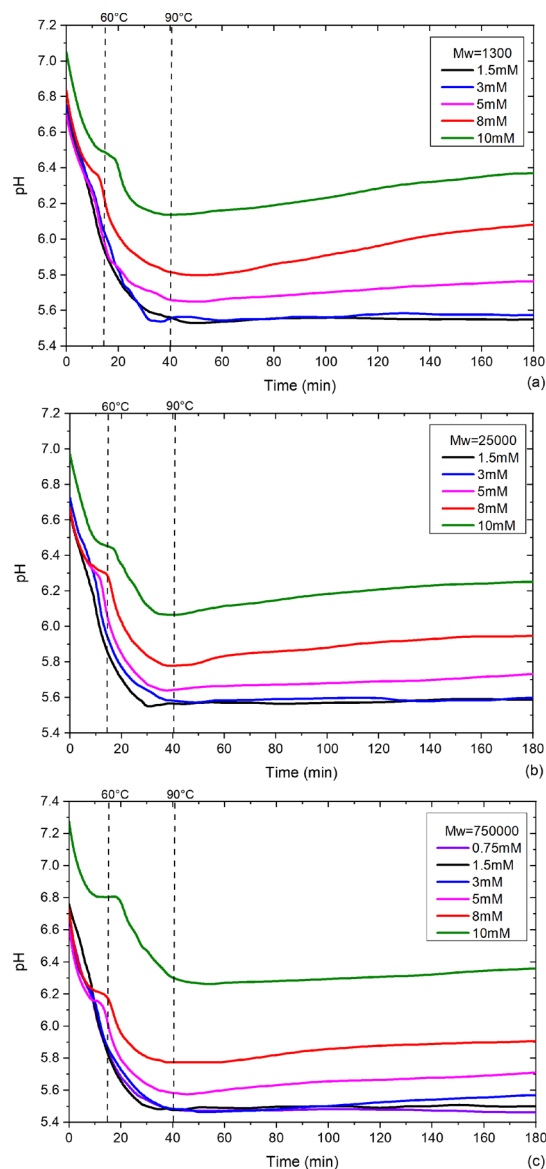


Figure 3. Evolution of the pH during the growth as a function of time for the different PEI concentrations and for the given M_w of (a) 1300, (b) 25 000, and (c) 750 000.

somehow be hampered by the protonated PEI through repulsive electrostatic interactions, and its magnitude may depend on the PEI concentration and M_w .

More importantly, the pH is significantly higher as the PEI concentration is increased from 1.5 to 10 mM, owing to the number of side amino groups, regardless of its M_w . The increase in the length of ZnO NWs in the low PEI concentration range is certainly related to the drastic decrease in the homogeneous nucleation in aqueous solution at the benefit of the heterogeneous nucleation, which originates from the presumable coordination of PEI with the Zn(II) ions. In contrast to the only case of HMTA in ref 9, the growth of ZnO NWs is here almost exclusively driven by the heterogeneous nucleation. As the PEI concentration is further increased, it is expected that the solubility is increased, by analogy with the thermodynamic simulations in ref 20, considering the addition of ammonia with a different volume. This may in turn decrease the supersaturation, progressively reducing the length of ZnO NWs. The evolution of the length of ZnO NWs and,

correlatively, of its volume as a function of the PEI concentration and of its M_w is thus governed mainly by the presumable formation of PEI–Zn(II) ion complexes suppressing the homogeneous nucleation and by the different supersaturation levels depending on the pH.

Effects of PEI on the Diameter of ZnO NWs. The evolution of the diameter of ZnO NWs as a function of the PEI concentration for the given M_w of 1300, 25 000, and 750 000 is presented in Figure 2b. As the PEI concentration is increased from 0 to 3 mM, the diameter of ZnO NWs drastically decreases from 70 ± 3 to about 50 nm, regardless of the M_w . The present decrease in the diameter of ZnO NWs correlated with the concomitant drastic increase in their length results in a significant increase in their aspect ratio, as presented in Figure 2c. This unambiguously indicates that PEI inhibits the development of the sidewalls of ZnO NWs and thus limits their radial growth, even in the present low pH range. The decrease in the diameter is much less pronounced as the PEI concentration is further increased from 3 to 10 mM, and the diameter eventually saturates down to 42 ± 3 , 45 ± 3 , and 53 ± 3 nm for the given M_w of 1300, 25 000, and 750 000, respectively. A further increase in the aspect ratio can be achieved by prolonging the growth time, increasing the solution volume in the sealed beaker, or varying the concentration ratio between zinc nitrate and HMTA.

The Raman spectra of the as-grown and annealed ZnO NWs at 300 °C for 30 min under nitrogen atmosphere are presented in Figure 4. On both Raman spectra, the lines pointing at 1295

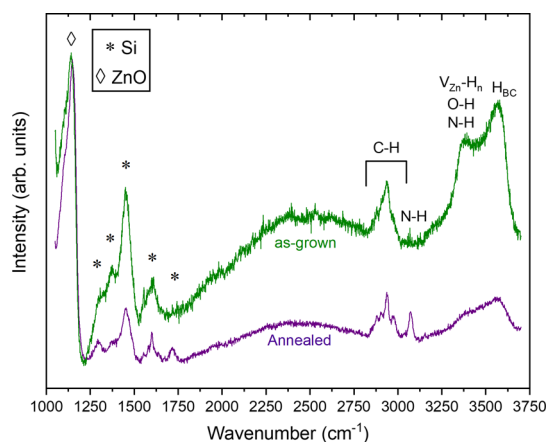


Figure 4. Raman spectra of as-grown and annealed ZnO NWs at 300 °C for 30 min under nitrogen atmosphere using the PEI concentration and M_w of 3 mM and 1300, respectively.

(2TO + TA), 1373 (2TO + TA), 1450 (3TO), 1553 (3TO), and 1600 cm^{-1} (3TO) are assigned to the modes of the silicon substrate.⁴⁵ The Raman line at 1145 cm^{-1} is assigned to a ZnO second-order mode.⁴⁶ Interestingly, a vast number of Raman lines attributed to the antisymmetric and symmetric stretching modes of the C–H_x groups occurs in the range of 2800–3000 cm^{-1} , specifically pointing at 2880, 2907, 2936, and 2974 cm^{-1} .⁴⁷ These modes were previously associated with the presence of residual HMTA molecules, following their adsorption on the sidewalls of ZnO NWs.⁹ In contrast, they are also very likely here the signature of residual PEI molecules, following their adsorption on the sidewalls of ZnO NWs. Correlatively, an additional Raman line around 3070 cm^{-1} is attributed to the stretching N–H modes.^{48,49} This is also

related to the residual PEI molecules, as the present line is typically not reported on the Raman spectra of HMTA.⁹ Its intensity further increases after annealing under nitrogen atmosphere at 300 °C for 1 h. It should further be noted that the C–N–C, C–H, and C–H₂ modes in the range of 1000–1500 cm^{-1} may occur, but the related Raman lines cannot be distinguished owing to the presence of the silicon and ZnO modes in the same range of wavenumbers. Eventually, two broad Raman lines arise at 3388 and 3570 cm^{-1} . The more intense Raman line at 3570 cm^{-1} is related to interstitial hydrogen in bond-centered sites (H_{BC}).^{50,51} The less intense Raman line at 3388 cm^{-1} is expected to involve a larger number of contributions, originating from the O–H bonds on the surface of ZnO NWs,^{48,50} as well as from the hydrogen-related species such as defect complexes involving multiple O–H bonds in a zinc vacancy in the form of (V_{Zn} –H_n), where n lies in the range of 2–4.^{50,52,53} As discussed in ref 54, the intensity of the present two broad Raman lines is strongly decreased as the annealing temperature is raised to 300 °C and ends up vanishing at 500 °C. In the present case involving the addition of PEI, it is also likely that stretching N–H modes occur in the present Raman line, as shown in ref 55 reporting the adsorption of NH₃ on TiO₂ nanoparticles. Overall, the present Raman scattering analysis supports the adsorption of PEI on the sidewalls of ZnO NWs, mainly through the presence of C–H_x and N–H modes.

Effects of PEI on the Apparent Density of ZnO NWs.

The evolution of the apparent density of ZnO NWs as a function of the PEI concentration for the given M_w of 1300, 25 000, and 750 000 is presented in Figure 5. Whatever the PEI

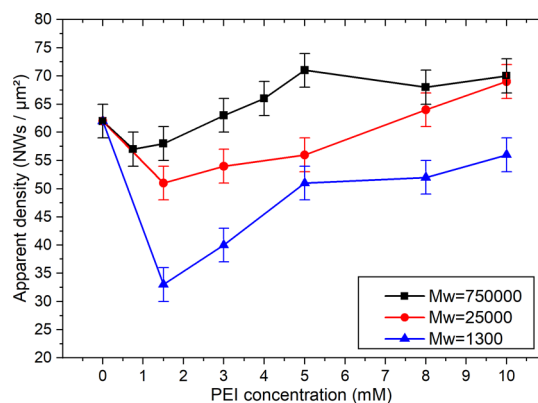


Figure 5. Evolution of the apparent density of ZnO NWs grown by CBD as a function of the PEI concentration and for the given M_w of 1300, 25 000, and 750 000.

concentration, the apparent density of ZnO NWs is much smaller than the density of the *c*-axis-oriented ZnO nanoparticles, which is typically larger than 100 μm^{-2} , as deduced from the FESEM image analysis and X-ray diffraction measurements following the procedure described in ref 9. As the PEI concentration is increased from 0 to 1.5 mM, the apparent density of ZnO NWs is significantly decreased from 62 ± 3 to 57 ± 3 , 51 ± 3 , and 33 ± 3 μm^{-2} for the given M_w of 750 000, 25 000, and 1300, respectively. The present decrease in the apparent density of ZnO NWs is not related to the variation of the magnitude of coalescence process given that the length of ZnO NWs is concomitantly increased strongly while their diameter is progressively decreased. Instead, it is expected that PEI affects the nucleation process of ZnO NWs

on the ZnO seed layer by presumably adsorbing on the ZnO nanoparticles oriented with the nonpolar *m*-planes parallel to the surface. The present adsorption may reduce the nucleation rate of ZnO NWs on ZnO nanoparticles with the semipolar or polar *c*-planes parallel to the surface acting as nucleation sites by steric hindrance. Also, the verticality of ZnO NWs was assessed by X-ray pole figures recorded on the (0002) diffraction peak by measuring the corresponding full width at half-maximum (fwhm), as presented in Figure 6. The ZnO

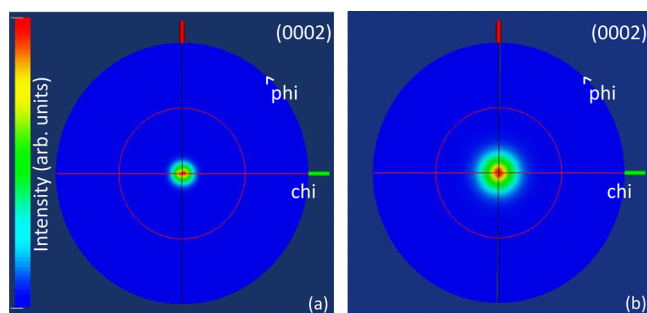


Figure 6. Typical X-ray pole figures recorded on the symmetric (0002) diffraction peak of ZnO NWs grown by CBD with (a) no PEI and (b) a PEI M_w and concentration of 1300 and 1.5 mM, respectively.

NWs grown with no PEI have a typical mean tilt angle of 5–10°. The addition of PEI is associated with a systematic vertical misalignment of ZnO NWs, which exhibit a larger mean tilt angle lying in the range of 10–25°. This may be an additional indication for the effect of PEI on the nucleation process. Moreover, the magnitude of the present process may also be affected by the M_w . As the PEI concentration is further increased from 3 to 10 mM, the apparent density continuously increased to 56 ± 3 , 69 ± 3 , and $70 \pm 3 \mu\text{m}^{-2}$ for the given M_w of 1300, 25 000, and 750 000, respectively. This increase is, to some extent, related to the decrease in the length and diameter of ZnO NWs, reducing in turn the magnitude of the

coalescence process. This arises mainly from the vertical misalignment of ZnO NWs, resulting in an apparent density depending on the height at which it is measured.

DISCUSSION

The different roles of PEI as well as the effects of its M_w (i.e., chain length) are summarized in Figure 7. The addition of PEI has a strong influence on the growth regime, suppressing the homogeneous growth in aqueous solution via the presumable formation of PEI–Zn(II) ion complexes at the benefit of the heterogeneous growth of ZnO NWs on the polycrystalline ZnO seed layer. This is favorable for the elongation of ZnO NWs, and hence their length drastically increases with the addition of PEI and as its concentration is slightly increased. Further, the addition of PEI modifies the pH, directly affecting the supersaturation level in aqueous solution. As the PEI concentration is further increased, the supersaturation level basically decreases, further reducing the length of ZnO NWs. It is also very likely that the presence of protonated PEI with a positive charge affects the diffusive transport of Zn(II) ions by repulsive electrostatic interactions. The addition of PEI also inhibits the development of the sidewalls of ZnO NWs, reducing the radial growth and their related diameters. PEI is thus expected to adsorb on the nonpolar *m*-plane sidewalls of ZnO NWs, even at the low pH range investigated here. The adsorption process of PEI is still under debate; however, electrostatic interactions are ruled out in the present investigation, in which a large part of PEI is protonated and thus positively charged in the low pH range, while the *m*-plane sidewalls are positively charged as well below the IEP. Alternative adsorption mechanisms involving the formation of covalent and hydrogen bonding with atoms and/or defects at the surface for instance may proceed. Eventually, PEI clearly affects the nucleation process of ZnO NWs by presumably adsorbing on the ZnO nanoparticles oriented with the nonpolar *m*-planes parallel to the surface, reducing in turn their nucleation rate and inducing a strong vertical misalignment. Owing to their pronounced chain length, steric

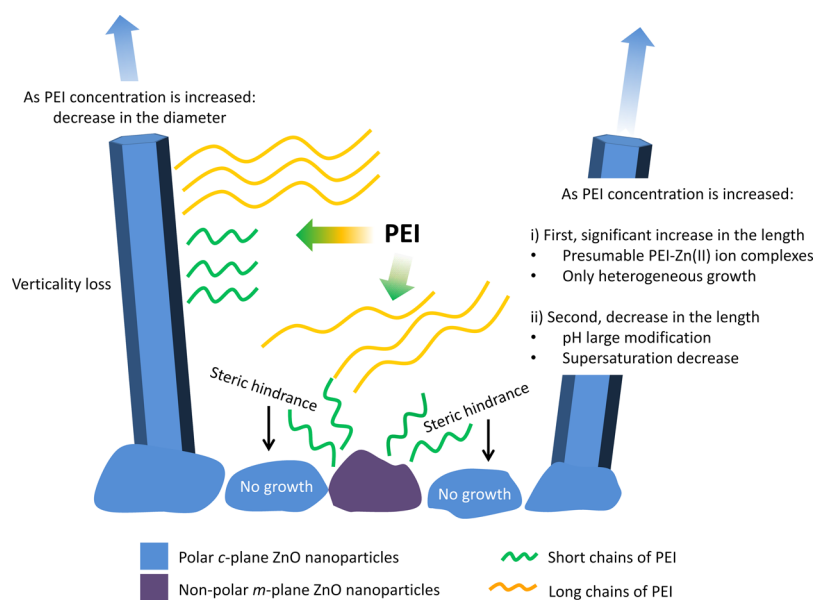


Figure 7. Schematic recapitulating the different roles of PEI and the effects of its M_w (i.e., chain length) on the nucleation and growth of ZnO NWs by CBD.

hindrance may occur and directly disturb the nucleation process of ZnO NWs.

CONCLUSIONS

In summary, the multiple roles of PEI in the growth of ZnO NWs by CBD have thoroughly been investigated by disentangling their effects from the effects of ammonia and by simultaneously varying its M_w and concentration over a broad range of 1300–750 000 and of 1.5–10 mM, respectively. It is shown that the addition of PEI significantly increases the aspect ratio of ZnO NWs by favoring their elongation along the polar c -axis and by inhibiting the development of their sidewalls. As the PEI concentration is increased, the aspect ratio of ZnO NWs is initially increased significantly and then saturates or decreased, depending on its M_w . The length of ZnO NWs is basically improved initially by suppressing the homogeneous growth at the benefit of the heterogeneous growth via the presumable formation of PEI–Zn(II) ion complexes. It is then decreased by the change of the supersaturation level through the pH modification that is dependent upon the PEI M_w and concentration. Correlatively, the inhibition of the development of the sidewalls of ZnO NWs is achieved by the PEI adsorption on their nonpolar m -planes, as further supported by the Raman scattering analysis showing the occurrence of modes attributed to the C–H_x and N–H groups. The adsorption operates even in the present low pH range, which somehow rules out the present involvement of electrostatic interactions as the dominant mechanism. Importantly, the addition of PEI drastically affects the density of ZnO NWs and hence their nucleation process on the polycrystalline ZnO seed layer by presumably adsorbing on the nanoparticles oriented with the m -planes parallel to the surface. The present adsorption typically reduces the nucleation rate of ZnO NWs and induces a strong vertical misalignment, presumably via steric hindrance, whereas its magnitude highly depends on the PEI M_w . These findings reveal the multiple roles of PEI in the growth of ZnO NWs by CBD, which are essential for the improvement of the overall performances of the related nanoscale engineering devices.

EXPERIMENTAL SECTION

The 30 nm thick polycrystalline ZnO seed layers were deposited by the sol–gel process using dip coating on top of the (0001) Si wafer cleaned by an ultrasonic bath with acetone and isopropanol. The solution of chemical precursors was composed of 375 mM of zinc acetate dihydrate (Zn(CH₃COO)₂·2H₂O) mixed with 375 mM of monoethanolamine in pure ethanol. It was stirred on a hot plate kept at 60 °C for a couple of hours and then at room temperature for 24 h. The samples were slowly dipped and gently pulled out at a withdrawal speed of 3.3 mm/s under controlled atmosphere with a hygrometry lower than 15%. They were further annealed on a hot plate kept at 300 °C for 10 min for evaporating the residual organic compounds and then at 500 °C for 1 h for crystallization. The growth of ZnO NW arrays was performed by CBD using an aqueous solution containing 25 mM of zinc nitrate hexahydrate (Zn(NO₃)₂·6H₂O) and 25 mM of HMTA. The samples were put horizontally face down in a sealed beaker within a regular oven kept at 90 °C for 3 h. The solution temperature was thus raised progressively to 90 °C within 40 min. PEI in its branched form and with the M_w of 1300, 25 000, and 750 000 was added, with the concentration

ranging from 1.5 to 10 mM. These M_w values correspond to the so-called short, medium, and long chains, respectively, roughly varying from a few micrometers to more than 1 nm through several tens of micrometers.

The in situ pH measurements were performed during the CBD of ZnO NWs using the InLab Versatile Pro pH electrode from Mettler Toledo, whereas the temperature was recorded with a temperature probe combined with the present pH electrode. The top-view and cross-sectional FESEM images were recorded with an FEI Quanta 250 field emission gun scanning electron microscope to investigate the morphological properties of ZnO NWs (i.e., vertical alignment, typical dimensions like length and diameter, and density). Raman scattering was performed with a Jobin Yvon/HORIBA Labram spectrometer equipped with a liquid nitrogen-cooled charge-coupled device detector. The 488 nm excitation line of an Ar⁺ laser was used, and the power at the sample surface was close to 3.75 mW. The light was focused on a spot size smaller than 1 μm² using a 50 times long working distance objective. The Raman spectra were calibrated using a silicon reference sample at room temperature with a theoretical position of 520.7 cm^{−1}. The X-ray pole figures were obtained with a Siemens D5000 diffractometer using Cu K_{α1} radiation. The apparatus was equipped with a four-circle goniometer (i.e. ω , 2θ , φ , and χ), 2.5° Sollers slits, as well as a graphite monochromator and a scintillation detector. The complete X-ray pole figure patterns were first recorded on the (0002) diffraction peak and the second rebuilt for a χ angle in the range of −90 to +90°. For positive and negative χ angles, the intensity was obtained by integrating the corresponding intensity for the φ angle in the range of 0–180° and 180–360°, respectively. Half of fwhm represents a quantitative measurement of the mean tilt angle of ZnO NWs.

ASSOCIATED CONTENT

Supporting Information

The Supporting Information is available free of charge on the ACS Publications website at DOI: 10.1021/acsomega.8b01641.

Cross-sectional view and top-view FESEM images of ZnO NWs grown by CBD with a PEI concentration in the range of 1.5–10 mM and for a given M_w of 25 000 and cross-sectional view and top-view FESEM images of ZnO NWs grown by CBD with a PEI concentration in the range of 0.75–8 mM and for a given M_w of 750 000 (PDF)

AUTHOR INFORMATION

Corresponding Author

*E-mail: vincent.consonni@grenoble-inp.fr.

ORCID

Vincent Consonni: 0000-0003-0171-8746

Notes

The authors declare no competing financial interest.

ACKNOWLEDGMENTS

This work was supported by the LabEx Cemam under the contract ANR-10-LABX-44-01 and by the French Research National Agency through the projects DOSETTE (ANR-17-CE24-0003) and ROLLER (ANR-17-CE09-0033). R.P. held a doctoral fellowship from the LabEx Cemam. This research has

further benefited from the characterization equipment of the Grenoble INP—CMTC platform. Funding by Cross-Disciplinary Program of the IDEX Université Grenoble Alpes under Contract ANR-15-IDEX-02 through Project ECO-SESA is also acknowledged.

REFERENCES

- (1) Vayssieres, L.; Keis, K.; Lindquist, S.-E.; Hagfeldt, A. Purpose-Built Anisotropic Metal Oxide Material: 3D Highly Oriented Microrod Array of ZnO. *J. Phys. Chem. B* **2001**, *105*, 3350–3352.
- (2) Xu, S.; Wang, Z. L. One-Dimensional ZnO Nanostructures: Solution Growth and Functional Properties. *Nano Res.* **2011**, *4*, 1013–1098.
- (3) Guillemin, S.; Consonni, V.; Appert, E.; Puyoo, E.; Rapenne, L.; Roussel, H. Critical Nucleation Effects on the Structural Relationship Between ZnO Seed Layer and Nanowires. *J. Phys. Chem. C* **2012**, *116*, 25106–25111.
- (4) Wei, Y.; Wu, W.; Guo, R.; Yuan, D.; Das, S.; Wang, Z. L. Wafer-Scale High-Throughput Ordered Growth of Vertically Aligned ZnO Nanowire Arrays. *Nano Lett.* **2010**, *10*, 3414–3419.
- (5) Consonni, V.; Sarigiannidou, E.; Appert, E.; Bocheux, A.; Guillemin, S.; Donatini, F.; Robin, I.-C.; Kioseoglou, J.; Robaut, F. Selective Area Growth of Well-Ordered ZnO Nanowire Arrays with Controllable Polarity. *ACS Nano* **2014**, *8*, 4761–4770.
- (6) Greene, L. E.; Law, M.; Tan, D. H.; Montano, M.; Goldberger, J.; Somorjai, G.; Yang, P. General Route to Vertical Nanowire Arrays Using Textured ZnO Seeds. *Nano Lett.* **2005**, *5*, 1231–1236.
- (7) Guillemin, S.; Appert, E.; Roussel, H.; Doisneau, B.; Parize, R.; Boudou, T.; Bremond, G.; Consonni, V. Controlling the Structural Properties of Single Step, Dip Coated ZnO Seed Layers for Growing Perfectly Aligned Nanowire Arrays. *J. Phys. Chem. C* **2015**, *119*, 21694–21703.
- (8) Cossuet, T.; Roussel, H.; Chauveau, J. M.; Chaix-Pluchery, O.; Thomassin, J. L.; Appert, E.; Consonni, V. Well-Ordered ZnO Nanowires with Controllable Inclination on Semipolar ZnO Surfaces by Chemical Bath Deposition. *Nanotechnology* **2018**, *29*, 475601.
- (9) Parize, R.; Garnier, J.; Chaix-Pluchery, O.; Verrier, C.; Appert, E.; Consonni, V. Effects of Hexamethylenetetramine on the Nucleation and Radial Growth of ZnO Nanowires by Chemical Bath Deposition. *J. Phys. Chem. C* **2016**, *120*, 5242–5250.
- (10) McPeak, K. M.; Becker, M. A.; Britton, N. G.; Majidi, H.; Bunker, B. A.; Baxter, J. B. In Situ X-ray Absorption Near-Edge Structure Spectroscopy of ZnO Nanowire Growth During Chemical Bath Deposition. *Chem. Mater.* **2010**, *22*, 6162–6170.
- (11) Law, M.; Greene, L. E.; Johnson, J. C.; Saykally, R.; Yang, P. Nanowire Dye-Sensitized Solar Cells. *Nat. Mater.* **2005**, *4*, 455–459.
- (12) Qiu, J.; Li, X.; Zhuge, F.; Gan, X.; Gao, X.; He, W.; Park, S.-J.; Kim, H.-K.; Hwang, Y.-H. Solution-derived 40 μm vertically aligned ZnO nanowire arrays as photoelectrodes in dye-sensitized solar cells. *Nanotechnology* **2010**, *21*, 195602.
- (13) Xu, C.; Shin, P.; Cao, L.; Gao, D. Preferential Growth of Long ZnO Nanowire Arrays and Its Application in Dye-Sensitized Solar Cells. *J. Phys. Chem. C* **2010**, *114*, 125–129.
- (14) Liu, B.; Zeng, H. C. Hydrothermal synthesis of ZnO nanorods in the diameter regime of 50 nm. *J. Am. Chem. Soc.* **2003**, *125*, 4430–4431.
- (15) Govender, K.; Boyle, D. S.; Kenway, P. B.; O'Brien, P. Understanding the Factors that Govern the Deposition and Morphology of Thin Films of ZnO from Aqueous Solution. *J. Mater. Chem.* **2004**, *14*, 2575–2591.
- (16) Xu, L.; Guo, Y.; Liao, Q.; Zhang, J.; Xu, D. Morphological Control of ZnO Nanowires by Electrodeposition. *J. Phys. Chem. B* **2005**, *109*, 13519–13522.
- (17) Tian, Z. R.; Voigt, J. A.; Liu, J.; McKenzie, B.; McDermott, M. J. Biomimetic Arrays of Oriented Helical ZnO Nanorods and Columns. *J. Am. Chem. Soc.* **2002**, *124*, 12954–12955.
- (18) Kim, J. H.; Andeen, D.; Lange, F. F. Hydrothermal Growth of Periodic, Single-Crystal ZnO Microrods and Microtunnels. *Adv. Mater.* **2006**, *18*, 2453–2457.
- (19) Joo, J.; Chow, B. Y.; Prakash, M.; Boyden, E. S.; Jacobson, J. M. Face-Selective Electrostatic Control of Hydrothermal Zinc Oxide Nanowire Synthesis. *Nat. Mater.* **2011**, *10*, 596–601.
- (20) Verrier, C.; Appert, E.; Chaix-Pluchery, O.; Rapenne, L.; Raffay, Q.; Kaminski-Cachopo, A.; Consonni, V. Effects of the pH on the Formation and Doping Mechanisms of ZnO Nanowires Using Aluminum Nitrate and Ammonia. *Inorg. Chem.* **2017**, *56*, 13111–13122.
- (21) Verrier, C.; Appert, E.; Chaix-Pluchery, O.; Rapenne, L.; Raffay, Q.; Kaminski-Cachopo, A.; Consonni, V. Tunable Morphology and Doping of ZnO Nanowires by Chemical Bath Deposition Using Aluminum Nitrate. *J. Phys. Chem. C* **2017**, *121*, 3573–3583.
- (22) Smits, R. G.; Koper, G. J. M.; Mandel, M. The Influence of Nearest- and Next-Nearest-Neighbor Interactions on the Potentiometric Titration of Linear Poly(ethylenimine). *J. Phys. Chem.* **1993**, *97*, 5745–5751.
- (23) Ziebarth, J. D.; Wang, Y. Understanding the Protonation Behavior of Linear Polyethylenimine in Solutions through Monte Carlo Simulations. *Biomacromolecules* **2010**, *11*, 29–38.
- (24) Sharma, K. P.; Choudhury, C. K.; Srivastava, S.; Davis, H.; Rajamohanam, P. R.; Roy, S.; Kumaraswamy, G. Assembly of Polyethylenimine in the Hexagonal Mesophase of Nonionic Surfactant: Effect of pH and Temperature. *J. Phys. Chem. B* **2011**, *115*, 9059–9069.
- (25) Choudhury, C. K.; Roy, S. Structural and dynamical properties of polyethylenimine in explicit water at different protonation states: a molecular dynamics study. *Soft Matter* **2013**, *9*, 2269–2281.
- (26) Kirby, G. H.; Cooley, K. M.; Armstrong, B. L. Tailored Rheological Behavior of Mullite and BSAS Suspensions Using a Cationic Polyelectrolyte. *Proceedings of GT2005*, 2005; p 68491.
- (27) Sun, C.; Tang, T.; Uludağ, H.; Cuervo, J. E. Molecular Dynamics Simulations of DNA/PEI Complexes: Effect of PEI Branching and Protonation State. *Biophys. J.* **2011**, *100*, 2754–2763.
- (28) Wu, W.; Hu, G.; Cui, S.; Zhou, Y.; Wu, H. Epitaxy of Vertical ZnO Nanorod Arrays on Highly (001)-Oriented ZnO Seed Monolayer by a Hydrothermal Route. *Cryst. Growth Des.* **2008**, *8*, 4014–4020.
- (29) Huang, Q.; Fang, L.; Chen, X.; Saleem, M. Effect of polyethylenimine on the Growth of ZnO Nanorod Arrays and their Application in Dye-Sensitized Solar Cells. *J. Alloys Compd.* **2011**, *509*, 9456–9459.
- (30) Choi, H.-S.; Vaseem, M.; Kim, S. G.; Im, Y.-H.; Hahn, Y.-B. Growth of high aspect ratio ZnO nanorods by solution process: Effect of polyethyleneimine. *J. Solid State Chem.* **2012**, *189*, 25–31.
- (31) Yin, X.; Que, W.; Fei, D.; Xie, H.; He, Z.; Wang, G. Strategies to Prepare an Efficient Photoanode for ZnO Nanowires-Based CdS-CdSe Co-Sensitized Solar Cells. *Electrochim. Acta* **2013**, *89*, 561–570.
- (32) Suresh, V.; Jayaraman, S.; Jailani, M. I. b. M.; Srinivasan, M. P. In Situ Application of Polyelectrolytes in Zinc Oxide Nanorod Synthesis: Understanding the Effects on the Structural and Optical Characteristics. *J. Colloid Interface Sci.* **2013**, *394*, 13–19.
- (33) Zhu, S.; Chen, X.; Zuo, F.; Jiang, M.; Zhou, Z.; Hui, D. Controllable synthesis of ZnO nanograss with different morphologies and enhanced performance in dye-sensitized solar cells. *J. Solid State Chem.* **2013**, *197*, 69–74.
- (34) Liu, K.; Wu, W.; Chen, B.; Chen, X.; Zhang, N. Continuous Growth and Improved PL Property of ZnO Nanoarrays with Assistance of Polyethylenimine. *Nanoscale* **2013**, *5*, 5986–5993.
- (35) Zhou, Y.; Wu, W.; Hu, G.; Wu, H.; Cui, S. Hydrothermal synthesis of ZnO nanorod arrays with the addition of polyethylenimine. *Mater. Res. Bull.* **2008**, *43*, 2113–2118.
- (36) Kim, K. S.; Jeong, H.; Jeong, M. S.; Jung, G. Y. Polymer-Templated Hydrothermal Growth of Vertically Aligned Single-Crystal ZnO Nanorods and Morphological Transformations Using Structural Polarity. *Adv. Funct. Mater.* **2010**, *20*, 3055–3063.

- (37) Chen, L.-Y.; Yin, Y.-T.; Chen, C.-H.; Chiou, J.-W. Influence of Polyethyleneimine and Ammonium on the Growth of ZnO Nanowires by Hydrothermal Method. *J. Phys. Chem. C* **2011**, *115*, 20913–20919.
- (38) Han, Z.; Li, S.; Chu, J.; Chen, Y. Controlled Growth of Well-Aligned ZnO Nanowire Arrays Using the Improved Hydrothermal Method. *J. Semicond.* **2013**, *34*, 063002.
- (39) Sun, X.; Li, Q.; Jiang, J.; Mao, Y. Morphology-Tunable Synthesis of ZnO Nanoforest and its Photoelectrochemical Performance. *Nanoscale* **2014**, *6*, 8769–8780.
- (40) Syrokostas, G.; Govatsi, K.; Yannopoulos, S. N. High-Quality, Reproducible ZnO Nanowire Arrays Obtained by a Multiparameter Optimization of Chemical Bath Deposition Growth. *Cryst. Growth Des.* **2016**, *16*, 2140–2150.
- (41) Takagishi, T.; Yoshikawa, K.; Hamano, H.; Kuroki, N.; Kozuka, H. Specific Interaction between Polyethylenimine and Azo Dyes Carrying Hydroxyl Groups. *J. Polym. Sci.* **1985**, *23*, 37–47.
- (42) Bencini, A.; Bianchi, A.; Garcia-España, E.; Micheloni, M.; Ramirez, J. A. Proton coordination by polyamine compounds in aqueous solution. *Coord. Chem. Rev.* **1999**, *188*, 97–156.
- (43) Cheng, J. J.; Nicaise, S. M.; Berggren, K. K.; Gradečak, S. Dimensional Tailoring of Hydrothermally Grown Zinc Oxide Nanowire Arrays. *Nano Lett.* **2016**, *16*, 753–759.
- (44) Cossuet, T.; Appert, E.; Thomassin, J.-L.; Consonni, V. Polarity-Dependent Growth Rates of Selective Area Grown ZnO Nanorods by Chemical Bath Deposition. *Langmuir* **2017**, *33*, 6269–6279.
- (45) Uchinokura, K.; Sekine, T.; Matsuura, E. Raman scattering by silicon. *Solid State Commun.* **1972**, *11*, 47–49.
- (46) Cuscó, R.; Alarcón-Lladó, E.; Ibáñez, J.; Artús, L.; Jiménez, J.; Wang, B.; Callahan, M. J. Temperature Dependence of Raman Scattering in ZnO. *Phys. Rev. B: Condens. Matter Mater. Phys.* **2007**, *75*, 165202.
- (47) Bertie, J. E.; Solinas, M. Infra-Red and Raman Spectra and the Vibrational Assignment of Hexamethylenetetramine- h_{12} and $-d_{12}$. *J. Chem. Phys.* **1974**, *61*, 1666–1677.
- (48) Reynolds, J. G.; Reynolds, C. L.; Mohanta, A.; Muth, J. F.; Rowe, J. E.; Everitt, H. O.; Aspnes, D. E. Shallow Acceptor Complexes in p-Type ZnO. *Appl. Phys. Lett.* **2013**, *102*, 152114.
- (49) Nickel, N. H.; Fleischer, K. Hydrogen Local Vibrational Modes in Zinc Oxide. *Phys. Rev. Lett.* **2003**, *90*, 197402.
- (50) Lavrov, E. V.; Weber, J.; Börrnert, F.; Van de Walle, C. G.; Helbig, R. Hydrogen-Related Defects in ZnO Studied by Infrared Absorption Spectroscopy. *Phys. Rev. B: Condens. Matter Mater. Phys.* **2002**, *66*, 165205.
- (51) Lavrov, E. V.; Börrnert, F.; Weber, J. Dominant Hydrogen-Oxygen Complex in Hydrothermally Grown ZnO. *Phys. Rev. B: Condens. Matter Mater. Phys.* **2005**, *71*, 035205.
- (52) Lee, J.-K.; Nastasi, M.; Hamby, D. W.; Lucca, D. A. Optical Observation of Donor-Bound Excitons in Hydrogen-Implanted ZnO. *Appl. Phys. Lett.* **2005**, *86*, 171102.
- (53) Herklotz, F.; Hupfer, A.; Johansen, K. M.; Svensson, B. G.; Koch, S. G.; Lavrov, E. V. Infrared Absorption on a Complex Comprising Three Equivalent Hydrogen Atoms in ZnO. *Phys. Rev. B: Condens. Matter Mater. Phys.* **2015**, *92*, 155203.
- (54) Cossuet, T.; Donatini, F.; Lord, A. M.; Appert, E.; Pernot, J.; Consonni, V. Polarity-Dependent High Electrical Conductivity of ZnO Nanorods and Its Relationship to Hydrogen. *J. Phys. Chem. C* **2018**, DOI: 10.1021/acs.jpcc.8b07388.
- (55) Pittman, R. M.; Bell, A. T. Raman Investigations of NH_3 Adsorption on TiO_2 , Nb_2O_5 , and Nb_2O_5/TiO_2 . *Catal. Lett.* **1994**, *24*, 1–13.